Journal of Food Engineering 365 (2024) 111824

Contents lists available at ScienceDirect

Journal of Food Engineering

journal homepage: www.elsevier.com/locate/jfoodeng

Band selection pipeline for maturity stage classification in bell peppers: From full spectrum to simulated camera data

J. Muñoz-Postigo [a], E.M. Valero [a], M.A. Martínez-Domingo [a,*], F.J. Lara [b], J.L. Nieves [a], J. Romero [a], J. Hernández-Andrés [a]

[a] Department of Optics, University of Granada, Campus Fuentenueva, s/n. 18071, Granada, Spain
[b] Department of Analytical Chemistry, University of Granada. Campus Fuentenueva, s/n. 18071, Granada, Spain

ARTICLE INFO

Keywords:
Bell peppers
Spectral imaging
Food engineering

ABSTRACT

This paper describes a workflow for classifying the maturity of bell peppers using hyperspectral imaging and machine learning. The approach involves using spectral reflectance to determine the number of maturity stages, followed by a classification task using the optimal bands for accurate classification. The study explores a realistic scenario using simulated camera responses and investigates the use of real sensors with their spectral sensitivities and noise. Four classifier algorithms (RBFNN, PLS-DA, SVM, and LDA) were employed to predict the maturity stage based on spectral reflectance. The best results were achieved with the LDA algorithm, which was used in the optimization process for band selection. The optimized bands in the VISNIR range (400–1000 nm) were found to be [783.5, 844.1, and 905.4] nm, with an accuracy of 90.67% for spectral data. For camera responses with intermediate-level noise, the best bands were [760, 820, and 900 nm], achieving an accuracy of 81%. Overall, using three bands yielded satisfactory and practical results for real-world implementation.

1. Introduction

Bell pepper is a widely cultivated vegetable typically measuring 6–9 cm wide and 7–10 cm in length. It has three or four distinct hulls and a thick flesh (3–7 mm). The pepper can be cut with or without a stalk and has a glossy exterior in various colors (green, red, yellow, or orange). It belongs to the Capsicum genus in the Solanaceae family, which encompasses approximately 2300 plant species, including the California variety (Bosland et al., 2012). They are rich in vitamin C, provitamin A and carotenoids (especially in the red varieties) (Howard et al., 1994).

Determining the quality and acceptability of bell peppers in the market relies on attributes such as firmness, maturity, weight, texture, decay incidence, and color (Weston and Barth, 1997). There is significant interest in developing non-destructive, environmentally friendly, and rapid methods for quality control. These methods encompass measurement of physical properties of bell peppers (Ignat et al., 2010; Mohebbi et al., 2012), spectroscopic measurements (Ignat et al., 2013), and more recently, hyperspectral imaging (Schmilovitch et al., 2014; Ignat et al., 2014; Paredes et al., 2019; Yuan et al., 2021; Logan et al., 2020; Babellahi et al., 2020). Ariyo et al. (2011) utilized discriminant analysis and classification methods to monitor the health status of bell peppers based on growth parameters measured six to ten weeks after transplanting, such as plant height, number of leaves, and fruit count. Ignat et al. (2013) utilized visible and near infrared spectrometry to estimate bell pepper chlorophyll and carotenoid content, important indicators of maturity and harvesting time. They successfully predicted these components using various regression algorithms, including kernel algorithm, partial least squares (PLSR), and support vector machine. Schmilovitch et al. (2014) used visible and near infrared hyperspectral imaging (550 nm–850 nm) to correlate with total soluble solids, total chlorophyll, carotenoid, and ascorbic acid content data of three bell pepper cultivars during a seven-week maturation period, and a similar strategy is found in Paredes et al. (2019). Ignat et al. (2014) used hyperspectral visible and infrared data along with multi-sensor data to predict the maturity of intact bell peppers. Logan et al. (2020) used visible and near infrared data to search for optimal wavelengths to predict the ripeness of different fruits including bell peppers. The search was performed with a genetic algorithm, and the prediction with convolutional neural networks. Babellahi et al. (2020) focused on the ability to differentiate between fresh and stored fruits, using ten selected wavelengths in the range 400–2500 nm. They also were able to detect chill injury and classify the fruit according to storage duration.

* Corresponding author.
E-mail address: martinezm@ugr.es (M.A. Martínez-Domingo).

https://doi.org/10.1016/j.jfoodeng.2023.111824
Received 3 July 2023; Received in revised form 13 October 2023; Accepted 5 November 2023
Available online 10 November 2023

Villaseñor-Aguilar et al.2020 (Villaseñor et al., 2020) evaluated bell pepper maturity using an artificial vision system based on RGB images, employing fuzzy logic models and deep learning algorithms. Althaus et al. (Althaus and Blanke, 2020) assessed bell pepper freshness by a profilometer, luster sensor, and light reflectance spectra with satisfactory results. Kasampalis et al. (2022) related the nutritional quality of bell peppers during harvest and subsequent storage with digital color imaging, chlorophyll fluorescence, and visible/near-infrared spectroscopy.

In summary, several of these studies (Ignat et al., 2013, 2014; Schmilovitch et al., 2014; Althaus and Blanke, 2020; Kasampalis et al., 2022), aim to correlate spectral measurements with chemical data or other physical magnitudes related to nutritional content or freshness of the peppers, while others use spectroscopic data or spectral reflectance in different ranges, selecting suitable wavelengths to predict the maturity stage (Ignat et al., 2014; Logan et al., 2020) or for other related purposes (Babellahi et al., 2020), or use conventional digital imaging sensor responses data for evaluating ripeness (Villaseñor et al., 2020). This study focus on the hyperspectral imaging technique, since it has been proven to facilitate the detection, classification, and visualization of quality and safety attributes of fruits and vegetables (Pu et al., 2015). The practical implementation of such a prediction system to be used as quality control would require using a monochrome sensor coupled with narrowband filters. None of the previous studies have tested the effect of the illumination, the filter transmittances, and the monochrome sensor responsivity on the task of classification of peppers according to their maturity stage.

In this study, the use of spectral reflectance in the visible and near infrared range is proposed to determine the appropriate number of maturity stage classes of bell peppers of three cultivars. Then, the identification of optimal spectral reflectance bands for achieving the highest classification rate, following the approach of previous authors (Logan et al., 2020; Babellahi et al., 2020). The additional contribution is that a realistic scenario was considered resembling a conveyor belt system where bell peppers are initially assessed after collection, as full reflectance hyperspectral capture is too slow for conveyor belt integration. To address this, the feasibility of using commercial filters coupled with a monochrome sensor was examined, considering their spectral transmittances, responsivity, simulated noise, for automated maturity assessment of bell peppers under a suitable artificial illumination light source. This pipeline is then intended to be incorporated into a quality check system acting once the peppers have been collected and before packaging, to prevent over-ripe fruits to be packaged and become spoiled during transport. The system studied improves pepper shelf-life assessment, ensuring better product quality for customers and proper harvesting by producers, ultimately boosting pepper market position and economic performance.

2. Materials and methods

2.1. Samples

Three varieties of bell pepper (Capsicum annuum) were collected by HORTOFRUTÍCOLA MABE S.A.T. cooperative in five different time intervals, starting from 155 DAA (Days After Anthesis). Gatherings 1–4 were one week apart (with gathering 1 corresponding to 162 DAA), and gathering 5 was two weeks after gathering 4 (corresponding to 207 DAA). The varieties collected were red (Hokkaido), orange (Denario), and yellow (Insignia). Each gathering included 10 peppers per variety, totaling 150 peppers for this study. The gathering commenced on March 15, 2022, and the peppers were cultivated in greenhouse environments across various locations in the province of Almeria, Spain. After the gathering, some samples were preserved at 8–12 °C for two additional weeks to observe the changes in their physical features such as color and firmness.

2.2. Assessment by chemical analysis

Half of the samples were randomly chosen for the measurement of Chlorophyll A, Chlorophyll B, and carotenoid contents, which are commonly used as chemical markers to assess the maturity stage of bell peppers (Ignat et al., 2013, 2014; Schmilovitch et al., 2014; Paredes et al., 2019). Two approximately 0.7 g samples were obtained from different parts of each pepper and immersed in 80% ethanol before being frozen overnight at −18 °C. The frozen tissue was then macerated in absolute ethanol, followed by centrifugation to separate the solid residue. The supernatant was filtered using glass-fiber syringe filters (13 mm, 1 μm) (VWR, USA), and a portion was transferred to a quartz cuvette for optical absorbance measurement. The absorbance was determined at 470, 648.6, and 664.2 nm using a spectrophotometer (Jenway 7205 UV/Visible, USA) as described by Ignat et al. (2013). The contents of Chlorophyll A, Chlorophyll B, Total Chlorophyll, and carotenoids were calculated using the equations proposed by (Lichtenthaler, 1987):

$$C_a(\mu g / mL) = 13.36A_{664.2} - 5.19A_{648.6} \quad (1)$$

$$C_b(\mu g / mL) = 27.43A_{648.6} - 8.12A_{664.2} \quad (2)$$

$$C_{a+b}(\mu g / mL) = 5.24A_{664.2} + 22.24A_{648.6} \quad (3)$$

$$C_c(\mu g / mL) = (1000A_{470} - 2.13C_a - 97.64C_b) / 209 \quad (4)$$

The chemical analysis results indicate a tendency of increasing carotenoid levels (with a less pronounced trend in the yellow variety) and decreasing total Chlorophyll levels as the bell peppers mature (Fig. 1). This observation aligns with previous studies on this species (Ignat et al., 2013; Althaus and Blanke, 2020; Kasampalis et al., 2022). The high standard deviation among peppers within each collection suggests that carotenoid and chlorophyll contents can vary among different plants or collection sites, making it challenging to directly utilize these chemical measurements for classifying the maturity stage in our case. The phenomenon of carotenoid and chlorophyll content variability in bell peppers across diverse cultivars and collection sites constitutes a well-established subject within the realm of plant biology and agricultural science. Multiple factors exert influence upon the chemical composition of bell peppers, encompassing genetic disparities among cultivars, environmental parameters, and agricultural methodologies. Notably, environmental variables, comprising temperature, light intensity, soil characteristics, and water availability, are recognized as pivotal determinants that exert a discernible impact on the chemical composition of bell peppers (Wall et al., 2001; León-Chan et al., 2017).

2.3. Hyperspectral data

The spectral reflectance of the samples was measured using a Spectronon PikaL camera (– Resonon), covering the range from 400 nm to 1000 nm with 150 spectral bands (visible and near infrared range, VISNIR). The camera, equipped with 900 pixels per line, captured images of the peppers placed on a linear stage. Illumination was provided by four halogen lamps (Fig. 2, left). Images were taken of all four faces of each pepper, and five samples were extracted from each face, avoiding specular reflection areas (Fig. 2, center).

Prior to every capture, a Teflon reference white (whose spectral reflectance is $W_{ref}(\lambda)$) was captured ($White(\lambda,x,y)$) as well as a dark image ($Black(\lambda,x,y)$) in order to perform flat field correction and dark noise subtraction. This way, spectral reflectance images ($Ref(\lambda,x,y)$) were obtained from the raw images ($Raw(\lambda,x,y)$) as shown in equation (5).

$$\mathrm{Ref}(\lambda,x,y) = (\mathrm{Raw}(\lambda,x,y) - \mathrm{Black}(\lambda,x,y)) / (\mathrm{White}(\lambda,x,y) - \mathrm{Black}(\lambda,x,y)) \cdot W_{\mathrm{ref}}(\lambda) \quad (5)$$

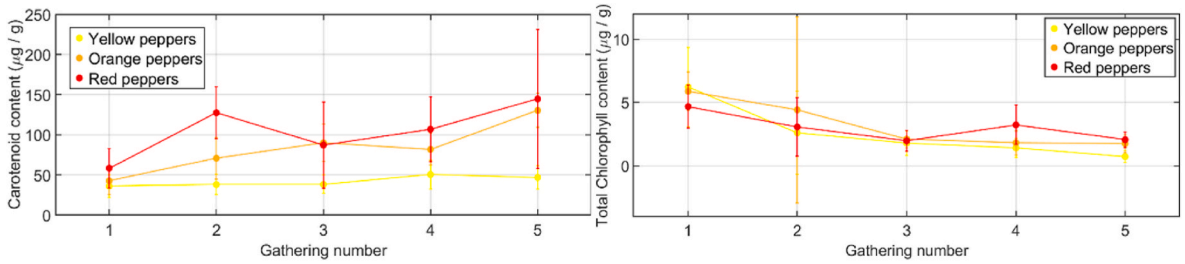

Fig. 1. Left: carotenoid content. Right: total chlorophyll (A + B), average values as a function of the gathering number (1: 162 DAA; 2: 169 DAA; 3: 176 DAA; 4: 183 DAA; 5:207 DAA). The error bars indicate one standard deviation.

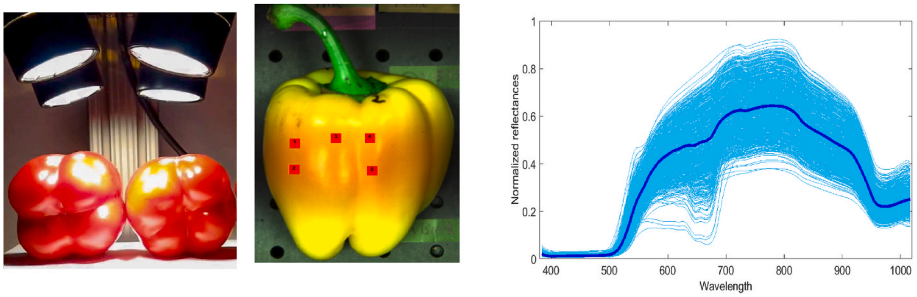

Fig. 2. Left: image capture setup with the illumination and the linear stage. Center: Example of camera response extraction in the VISNIR range. Right: spectral reflectances of the yellow variety set in the VISNIR range for all maturity stages. The mean spectral reflectance is shown in bold line.

Where x and y stand for pixel column and row respectively (spatial coordinates) and λ is the wavelength.

After some outlier data were discarded, a total of 2615 sample spectra were used for further analysis. In Fig. 2 right, the full set of spectra in the VISNIR range for the yellow variety is shown. They are similar to the spectra shown in (Logan et al., 2020).

2.4. Definition of the maturity stage classes

A statistical analysis using the Kolmogorov-Smirnov test was conducted on the extracted spectral reflectance data to determine significant differences between spectra collected at different times (G1 to G5). The samples from G1 and G2 did not show significant differences ($p = 0.28$), nor did the samples from G3 and G4 ($p = 0.34$). However, significant differences were observed between G2 and G3 samples ($p = 1.9e\text{-}9$), as well as between G4 and G5 samples ($p = 0.01$). Based on these findings, three maturity classes were defined: Class 1 (G1 + G2, representing early maturity), Class 2 (G3 + G4, representing medium maturity), and Class 3 (G5, representing advanced maturity). The data were labeled accordingly to create a ground truth for the maturity prediction classifier. The average reflectance for each maturity stage and pepper variety is shown in Fig. 3. Some samples in each group were stored at 4 °C for 14 days to observe the physical characteristics. Samples in G1 and G2 remained in good condition, maintaining firmness throughout the observation period. G3 and G4 samples started to lose firmness after 11–12 days of storage, while G5 samples lost firmness after 7 days. These results confirm the initial evaluation and classification of the samples based on maturity.

2.5. Classifier and optimization algorithms for band reduction

2.5.1. Classifier algorithms

Four classification algorithms were employed to predict the maturity class of the samples using the full spectral reflectance data. The algorithms used were Radial Basis Function Neuronal Network (RBFNN) (Beheim et al., 2004), Partial Least Squares Discriminant Analysis (PLS-DA) (Brereton and Lloyd, 2014), Support Vector Machine (SVM) (Weston and Watkins, 1998), and Linear Discriminant Analysis (LDA) (Fisher, 1936). These algorithms were chosen based on previous studies on bell peppers, although not specifically for maturity stage classification or prediction. The classification and optimization steps were performed using Matlab® code with functions from the Statistics and Machine Learning toolbox.

For the RBFNN and LDA algorithms, no data preprocessing was

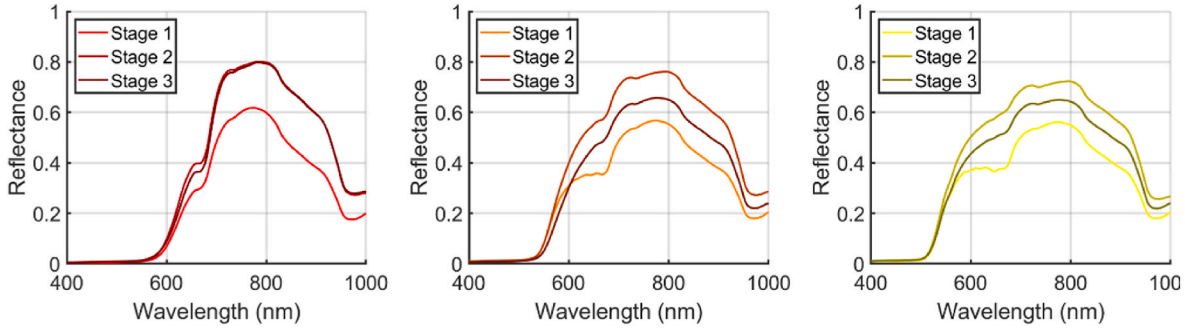

Fig. 3. Mean reflectance values of the samples corresponding to each of the three maturity stages or classes. Left column: Hokkaido (red variety); middle column: Denario (orange variety); right column: Insignia (yellow variety).

applied. However, for PLS-DA and SVM, z-score normalization was performed on the data. This normalization ensured that each spectrum and each band had a mean of 0 and a standard deviation of 1. The following equation was used for the normalization process.

$$Z = (x - \mu) \ / \sigma \tag{6}$$

where Z is the normalized value, X the original value, μ the mean of the data and σ the standard deviation.

The selected algorithms were evaluated using two strategies: 1) Confusion matrices were obtained by training the algorithms with 80% of the data and evaluating them on the remaining 20%. 2) Cross-validation was performed with k-fold (k = 5) to calculate the accuracy of the models.

Each classification algorithm underwent parameter optimization to achieve optimal results for our data. For LDA, default values were sufficient, and the fitcecoc Matlab® function with the Discriminant template was used. SVM required adjusting the Box Constraint parameter to 1000 for improved performance, compared to the default value of 1. RBFNN's spread parameter was crucial for classification, and values between 2 and 16 yielded the best results. The newrbe function in Matlab® was used, constructing a two-layered network with hidden neurons equal to the number of input vectors. PLS-DA implementation (Zontov et al., 2020) utilized the Matlab® GUI tool, with the soft version proving more effective. The number of components was optimized, and in our case, 20 components were chosen for the best results.

2.5.2. Band optimization algorithm

Optimal bands for maturity class prediction were determined using the LDA classifier with 5-fold cross-validation accuracy as the cost function. The Surrogate Optimization method (surrogateopt in Matlab®) (Gutmann, 2001), was employed to search for the best bands efficiently.

This iterative algorithm starts with random points within specified bounds and builds a surrogate model using radial basis function (RBF) interpolation. It then generates additional random points, evaluates a merit function based on the surrogate model and distances to previously evaluated points, and selects the best candidate point for evaluation of the original objective function. The process continues until a stopping criterion is met, such as reaching a maximum number of iterations.

In our case, the points evaluated correspond to different groups of one, two, or three bands within the measured spectrum. The algorithm aims to find the combination that minimizes the LDA classification error or maximizes accuracy.

To ensure robust results, the optimization was run 100 times, and the bands that appeared most frequently in the 100 runs were selected based on a histogram analysis.

By setting a maximum number of iterations, the execution time remained reasonable while still obtaining reliable results.

2.6. Camera capture simulation

It would be expected that the best bands identified using the full range of spectra may not be the best in real-life situations. This is because the actual capturing system used would be a simplified version, not a hyperspectral camera. Instead, it would consist of up to three monochrome sensors with narrowband filters attached to the camera lens. These different capture devices influence the input information for the classifier. Consequently, the optimization process to select the optimal spectral bands was re-run. This time, simulated camera responses were used based on the spectral reflectance multiplied by a real light source (color signal), the responsivity curve of a monochrome sensor, and a set of candidate filters. The camera response model includes both the illumination and sensor responsivity functions, specifically for a Silicon sensor. Gaussian distribution noise was also added, representing dark signal noise, at three levels: 1%, 3%, and 5% of the peak response (equivalent to approximately 40, 30, and 26 dB SNR). The illumination spectral power distribution from Thorlabs (Thorlabs), the spectral responsivity of the silicon sensor (from a Retiga 1300 Monochrome CCD camera), and the spectral transmittance of all candidate interference filters (a Vision Light Tech set) used in the optimization are shown in Fig. 4. It is assumed that the camera can provide RAW data because the sensor responses are linear with the received irradiance for most camera response values, given that the scene is properly exposed.

The camera response equation is:

$$\rho_{k,m} = \sum_{j=1}^{N} E_j R_{m,j} F_{k,j} S_j + \sigma_{k,m} \tag{7}$$

Where E_j is the SPD of the illumination shown in Fig. 3 left, $R_{m,j}$ is the spectral reflectance of the sample number m in band j, $F_{k,j}$ is the filter transmittance of filter number k in band j, S_j is the spectral responsivity function of the sensor in band j, and $\sigma_{k,m}$ is the added noise. By using this simplified model, the simulation of camera array responses closely approximates the response values of a real capture device used for on-site maturity stage prediction, compared to using spectral reflectance values alone. As mentioned earlier, it is not feasible to use a hyperspectral camera to capture and process the full spectrum in real-time applications involving a conveyor belt. Once the camera responses are obtained, the optimization process employs the Surrogated method and DA classifier to predict maturity classes using these camera responses. The results can then be analyzed to determine if the performance would be satisfactory in a more realistic scenario.

2.7. Workflow of the proposed pipeline for maturity stage classification

Fig. 5 illustrates a simplified workflow for designing an automatic classifier to determine the maturity stage of bell peppers. The process begins with capturing hyperspectral camera data, followed by defining the maturity stages based on the captured spectral information. Next, camera responses are calculated for each sample, candidate filter, sensor, and level of noise. Finally, a surrogate optimization algorithm is employed, using a DA-based classifier accuracy as the cost function, to identify the optimal spectral bands. Although bell peppers pose challenges in maturity stage prediction, a previous study (Logan et al., 2020) examines ripeness assessment within its context but also illustrates the potential applicability of the same workflow to a wide range of disparate species, including but not limited to potatoes, bananas, and peppers. This suggests that our proposed process can be adapted with minor adjustments for assessing the maturity stage of other species as well (see Fig. 6).

3. Results and discussion

3.1. Spectral reflectance data

3.1.1. Selection of the best classifier algorithm

As described in section 2.5.1, four classifier algorithms (RBFNN, PLS-DA, SVM, and DA) were utilized to generate initial results for predicting the maturity stage using the complete spectral reflectance data from the samples. This approach is anticipated to produce favorable outcomes based on previous studies (Ignat et al., 2013, 2014), but it does not reflect the practical aspects of automatically assessing the maturity of bell peppers after collection. Table 1 displays the overall accuracy of each algorithm for both spectral ranges, while Table 2 exhibits the confusion matrices specifically for cases where the total accuracy was less than 100%.

The RBFNN algorithm delivers the best overall results; however, considering factors such as parameterization, training process, and data preprocessing requirements, the LDA algorithm emerged as the preferable choice. This algorithm will be employed as the classifier in the cost function for the band selection optimization process (refer to section

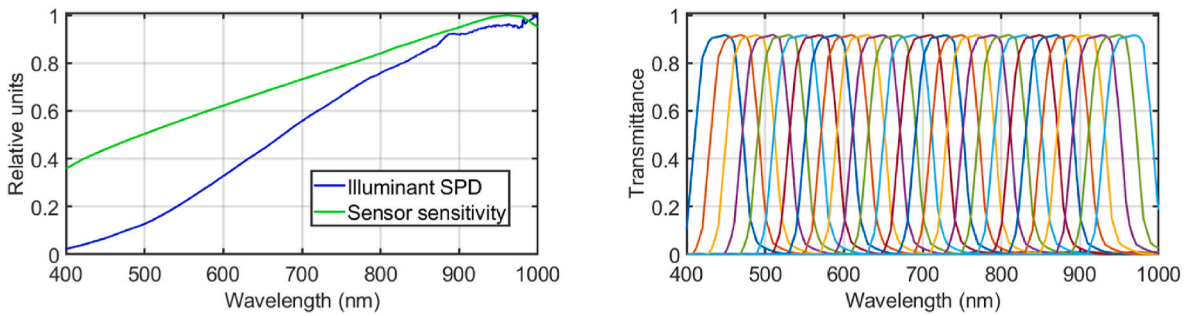

Fig. 4. Left: illumination SPD and sensors spectral responsivities (Retiga 1300 Monochrome camera for VISNIR range) Right: Vision Light Tech BP695 filters transmittances for the candidate filters used for the band selection optimization in the VISNIR range.

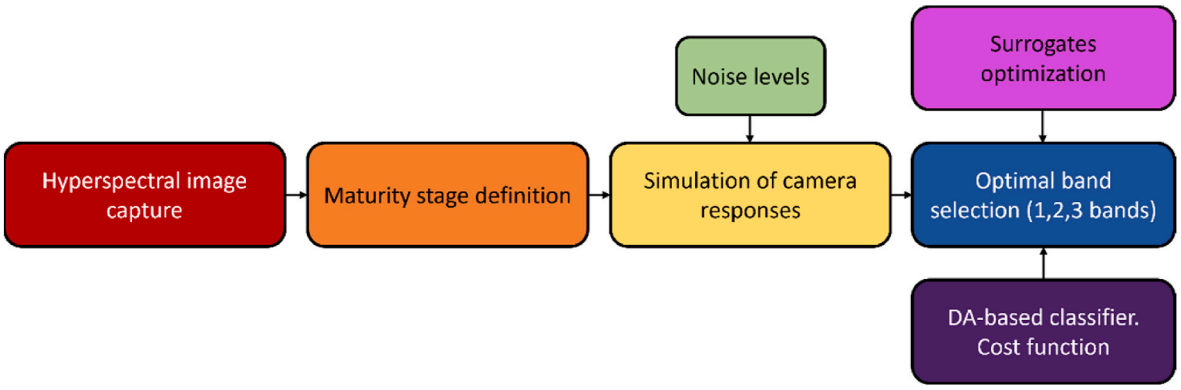

Fig. 5. Workflow of the complete proposed pipeline for maturity stage detection.

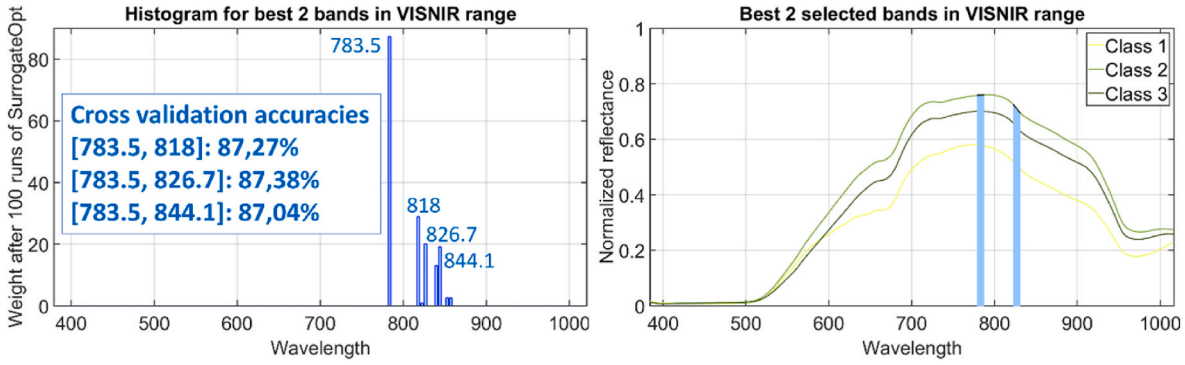

Fig. 6. Histograms of selected bands for the optimal two bands after 100 runs (left). Mean spectral reflectance of the three maturity classes with the two optimal bands highlighted (right).

Table 1
Total accuracy for the full spectra reflectance dataset maturity stage prediction.

Classifier algorithm	Accuracy
RBFNN	99.81%
PLS-DA	97.00%
SVM	99.69%
LDA	99.74%

3.2). It is worth noting that utilizing the full spectrum leads to excellent performance across all algorithms in the classification task, as anticipated. The accuracy obtained is similar or superior to the results of other studies using classification algorithms (Babellahi et al., 2020; Kasampalis et al., 2022), but a more detailed direct comparison is not possible due to differing input data or methodologies.

The data presented in Table 2, which includes the confusion matrices, confirms the accuracy of the tested classifiers. The data was split into 80% training and 20% testing sets to compute these matrices. Observing the confusion matrices, one can note that all errors occur between neighboring classes, predominantly classes 2 and 3. Therefore, the classifiers never mix up bell peppers that are highly mature with those that are very fresh, or vice versa.

3.1.2. *Optimal band selection*

In section 2.5.2, the LDA classifier accuracy served as the cost function for an optimization process that aimed to select the optimal combination of two and three bands. This optimization significantly reduces the computation time since there are typically millions of possible combinations when working with multiple bands. Surrogate optimization has been shown to converge to global minima when the cost function is suitably smooth, providing an additional advantage to

Table 2
Confusion matrices for those cases in which the accuracy did not reach 100%.

VISNIR													
RBFNN				PLS-DA			SVM			LDA			
	Predicted Classes			Predicted Classes			Predicted Classes			Predicted Classes			
Actual Classes	198	0	0	197	0	0	205	0	0	206	0	0	
	0	207	1	0	216	3	0	208	4	0	212	0	
	0	0	117	0	0	107	0	2	103	0	2	103	

this algorithm. However, in this case, the cost function was not evaluated with small enough steps to ensure its smoothness. Nonetheless, the achieved performance is satisfactory.

As a preliminary comparison, the maturity stage detection classifier was also run using the three channels of sRGB images of the samples, obtained from XYZ values using the standard transformation (Ohta and Robertson, 2006), as well as in the L*a*b* color space (CIE, 2007), computed from the reflectances under the D65 standard illumination. In the sRGB space, when separating the three varieties and conducting three independent classification processes, the highest mean accuracy achieved was 56.57%. When not separating by variety, the classifier achieved an accuracy of 41.57%, only marginally better than chance for a three-class classifier. In the L*a*b* space, when separating by variety, the average accuracy obtained was 72.0%, while the accuracy for the entire dataset was 60.19%. These classification results were based on the visible and near-infrared (VISNIR) spectral range, cropped at 700 nm due to the usage of color spaces.

Additionally, the performance was evaluated using data from individual bands. The best single band was found to be 901 nm, with an accuracy of 78.24%. Consequently, further improvement was anticipated by utilizing the optimization algorithm to determine the optimal combination of two and three bands.

3.1.2.1. Optimal two bands. As explained in section 2.5.2, the Surrogate optimization process was executed 100 times. After these runs, a histogram was created to display the frequency of each band being selected across the 100 iterations. The accuracy of the potential combinations involving the most frequently chosen bands was compared to determine the optimal pair. The pair [783.5, 826.7] nm yielded the best results, achieving a total accuracy of 87.38%.

As anticipated, using the optimal pair of bands resulted in higher accuracy compared to using a single band. Interestingly, the selected spectral locus for the optimal band pair is not in close proximity to the best individual band. This outcome is not surprising because when searching for an optimal pair of bands, the primary concern is the distinction in reflectance values between the two bands across different classes.

3.1.2.2. Optimal three bands. During the optimization process for selecting the best triplet of bands, the most favorable results were obtained with the triplet [783.5, 844.1, and 905.4] nm, achieving an accuracy of 90.67%. The use of three bands yields satisfactory outcomes and remains relatively feasible for implementation in real-life scenarios.

Fig. 7 displays the histograms and mean spectra with the optimal bands highlighted.

The optimal pair and optimal triplet share a common band (783.5 nm), which appeared most frequently in the search for the optimal pair. The closest band to this common member is not significantly distant from the second band in the optimal pair, but the third band is noticeably further apart. As shown in Fig. 7 (left), the optimal bands are positioned in a range where the separation between mean spectra corresponding to different maturity stages is more pronounced.

The accuracies achieved by the optimal triplets surpass those of the optimal pair, nearly approaching the values obtained with the full spectral data.

Implementing a real capture device using bands with peaks located similarly to the optimal bands would require incorporating one additional sensor compared to the two-band system. However, the improvement in accuracy might not justify the additional expense in this case. It is very difficult to compare our results with previous studies' data, because they either deal with correlation with chemical-physical measurements, or else they use a different number of bands or spectral range. Nevertheless, the 783.5 nm band found is within one of the sub-ranges highlighted by Kasamplis et al. (Kasampalis et al., 2022) (383–469, 555–595, 718–794, 940–1058,1402–1509, 1838–1930, 2511–2519 nm) as suitable for correlation with colorimetric data and use in classification of stored fruits maturity.

3.2. Simulated camera responses

3.2.1. Optimal band selection

3.2.1.1. Optimal single band. In this case, the quality surveillance system implementation involves only one sensor with a filter. The results can be found in Table 3 (rows 2–4). Although the optimal bands differ from those obtained for the full spectral reflectance scenario (section 3.1), the peak positions and accuracies are relatively close. The camera response simulation considers three additional factors that were not present in the spectral reflectance optimization: the illumination light source, interference filters, and noisy camera responses. However,

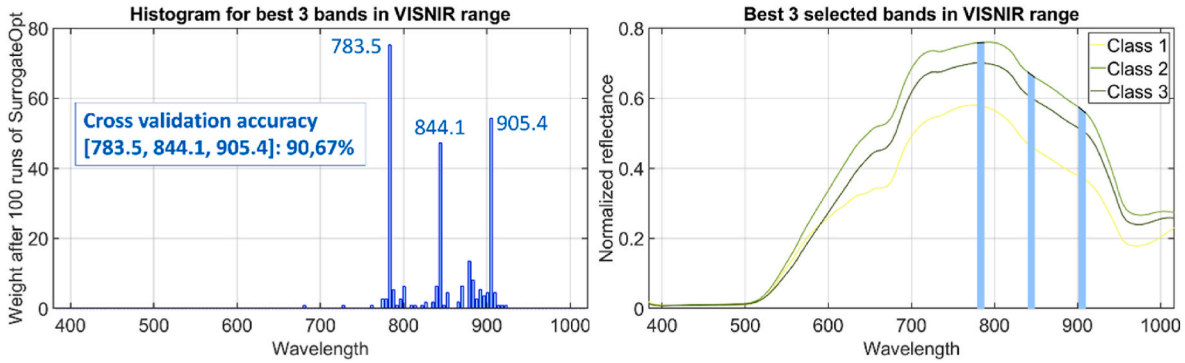

Fig. 7. Histograms of selected bands for the optimal triplets after 100 runs (left). Mean spectral reflectance of the three maturity classes with the three optimal bands highlighted (right).

Table 3
Optimal bands found for each noise level. N1 = single band. N2 = optimal pair. N3 = optimal triplet.

	VISNIR
N1 1% noise	[920] (77.97 %)
N1 3% noise	[900] (76.83 %)
N1 5% noise	[880] (75.91 %)
N2 1% noise	[780,880] (83.79%)
N2 3% noise	[760,880] (80.23%)
N2 5% noise	[880,920] (76.79%)
N3 1% noise	[440, 780,880] (84.05%)
N3 3% noise	[760, 880,900] (81.15%)
N3 5% noise	[760, 880,920] (78.32%)

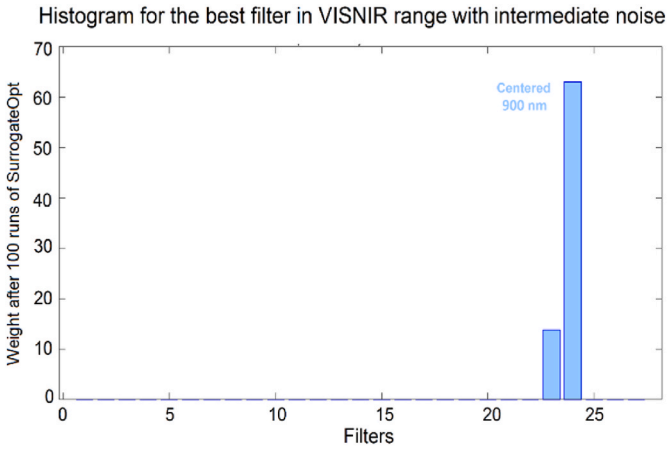

Fig. 8. Histograms of the selected single band after 100 runs with intermediate noise level camera responses.

despite these factors, the best band consistently tends to be around 900 nm. The presence of noise also affects the peak position of the optimal bands and the maximum accuracy achieved, as depicted in Table 3 (rows 2–4). As expected, the accuracy decreases as the noise level increases. Fig. 8 displays histograms for the optimization of a single band using camera responses with 3% noise (an intermediate noise level).

3.2.1.2. Optimal pairs and optimal triplets. The optimal band pairs and triplets (refer to Table 3, rows 5–7 for pairs, 8–10 for triplets) exhibit a similar pattern to the single band optimization. The selected bands are influenced by the level of noise, affecting both the peak position and the maximum accuracy achieved. Moreover, the peak positions differ from those obtained in the full spectral reflectance optimization, although they are relatively close for the 1% noise level. This underscores the significance of using accurate simulations as input for the optimization algorithms.

The accuracies obtained with the peak positions found in section 3.1 using spectral reflectance data, but with simulated camera responses, are lower compared to the optimal results obtained in section 3.2. This is due to the fact that the peak positions derived from spectral reflectance data are no longer optimal when a real device, illumination, and filters are employed for data collection.

Fig. 9 illustrates the histograms and optimal peak positions found for the intermediate noise simulation. Histograms of the selected optimal triplets of bands after 100 runs with intermediate noise level camera responses show that the three best filters are located at 900, 880 and 760 nm (Fig. 9, left). When only two filters were used, the best locations were around 880 and 760 nm (Fig. 9, right). As expected, the most successful ones are the ones located in the longer wavelengths of the studied spectral range.

As it was done in section 3.1.2, the RGB camera responses were simulated with the same illumination and the three levels of noise used in the camera simulations presented in this section. The simulated camera is a scientific RGB CCD camera (model Retiga RGB), and the

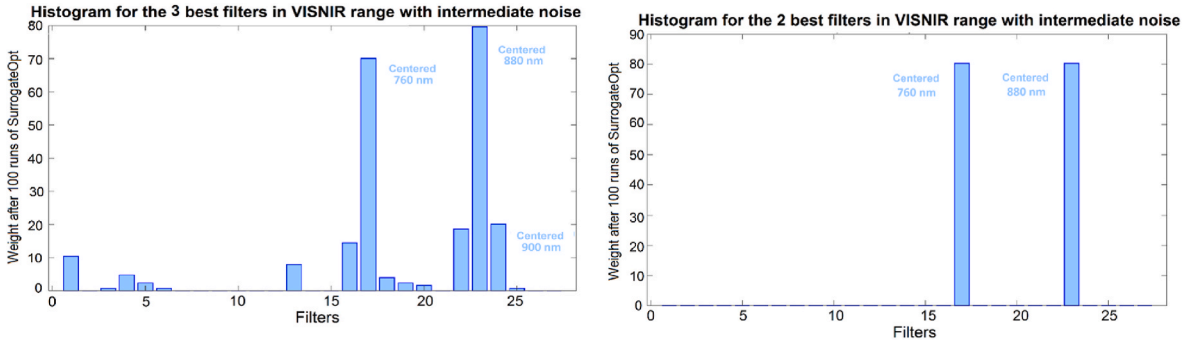

Fig. 9. Histograms of the selected optimal triplets of bands after 100 runs with intermediate noise level camera responses.

results range from 51.6% of accuracy for the noiseless case down to 46.0% for a 5% noise, using different classification models.

4. Conclusions

In this study, a complete pipeline that includes simulations of camera responses for the first time is presented to predict the maturity stage of bell peppers from different varieties. This is a significant issue for horticultural companies as they depend on timely harvesting to avoid losses caused by over-ripe peppers that are unsuitable for sale by the time they reach distributors or final sellers. The pipeline begins with capturing spectral reflectance data in the VISNIR range, which can also be obtained using area-based measurement devices. These data are used to define three maturity stages corresponding to different weeks after anthesis, starting from Day 162, which are validated by chemical measurements (chlorophyll and carotenoids content).

It is not possible to use the full reflectance spectrum in the quality assessment system, because of economical and capture time management reasons. Then, it is necessary to reduce the amount of information for the maturity stage prediction algorithm by finding optimal two or three bands that can achieve acceptable results in accuracy. On the other hand, none of the capture devices that could be used in this system directly provides spectral reflectance data. This would not be problematic if the peak positions of the optimal bands were the same for spectral reflectance data or the device camera responses. However, as it has been proven in this study, this is not the case. The results indicate that the optimal bands change when using camera responses as input data for the classifier. This suggests the crucial importance of using camera responses instead of reflectance data, which has not been explored in previous studies to our knowledge. The simulations consider noise, and as expected, the maximum accuracy achieved is highly dependent on the noise level of the capture system. The maximum modeled noise level in our study was 26 dB SNR. In practice, most current devices will have a SNR closer to 50 dB in average exposure and ISO settings. Under the maximum noise level, the accuracy reaches a minimum slightly below 80% for three filters.

Using this proposed pipeline, the number of filters can be adjusted based on the company's budget. They can choose simpler or more complex camera devices. The performance was examined with one to three filters, and the best results were obtained with three filters, although the difference between two and three filters is minimal. It would be advisable for any company willing to implement a maturity stage detection prediction to use their own illumination, capture device and filters to find the optimal spectral positions for their particular conditions. The peak positions provided in this study are strictly valid for the data used to obtain the simulated camera responses.

Additional limitations of this study are the sampling size (50 units per cultivar) which could partially limit the applicability of the findings; and the non-inclusion of noise impact reduction techniques in the camera responses simulations potentially has led to sub-optimal results in the 3% and 5% noise levels studied, and lack of real sensor responses data as input for the classifiers.

The outlined pipeline (excluding specific results shown) can be applied to any horticultural species that exhibits changes in spectral reflectance or fluorescence spectra depending on the maturity stage, although further effort could be needed to validate the method with field data from fruit packaging and distribution plants.

CRediT authorship contribution statement

J. Munoz-Postigo: Data curation, Software, Validation, Investigation. **E.M. Valero:** Conceptualization, Data curation, Formal analysis, Methodology, writing. **M.A. Martinez-Domingo:** Data curation, Formal analysis, Investigation, Methodology, Visualization, writing. **F.J. Lara:** Data curation, Formal analysis, Validation. **J.L. Nieves:** Conceptualization, Project administration, Resources, Supervision, writing. **J. Romero:** Conceptualization, Project administration, Resources, Supervision, writing. **J. Hernández-Andrés:** Conceptualization, Project administration, Resources, Supervision, writing, Funding acquisition.

Declaration of competing interest

The authors declare that they have no known competing financial interests or personal relationships that could have appeared to influence the work reported in this paper.

Data availability

Data will be made available on request.

Acknowledgements

The authors would like to thank the cooperative Hortofrutícola Mabe, S.A.T. for providing the samples for this study, as well as Professor Ana M. García-Campaña from Department of Analytical Chemistry from University of Granada, for her support and advice. Funding for open access charge: Universidad de Granada/CBUA.

References

Althaus, B., Blanke, M., 2020. Non-destructive, opto-electronic determination of the freshness and shrivel of Bell pepper fruits. J. Imaging 6 (11), 122. https://doi.org/10.3390/jimaging6110122.

Ariyo, O.S., Arogundade, O., Abdul-Rafiu, A.M., 2011. Discriminant and classification analysis of health status of bell pepper (Capsicum annuum). Res. J. Math. Stat. 3 (2), 77–81.

Babellahi, F., Paliwal, J., Erkinbaev, C., Amodio, M.L., Chaudhry, M.M.A., Colelli, G., 2020. Early detection of chilling injury in green bell peppers by hyperspectral imaging and chemometrics. Postharvest Biol. Technol. 162, 111100 https://doi.org/10.1016/j.postharvbio.2019.111100.

Beheim, L., Zitouni, A., Belloir, F., de la Housse, C.D.M., 2004. New RBF neural network classifier with optimized hidden neurons number. WSEAS Trans. Syst. 2, 467–472.

Bosland, P.W., Votava, E.J., Votava, E.M., 2012. Peppers: vegetable and spice capsicums 22. Cabi.

Brereton, R.G., Lloyd, G.R., 2014. Partial least squares discriminant analysis: taking the magic away. J. Chemometr. 28 (4), 213–225. https://doi.org/10.1002/cem.2609.

CIE (2007). Colorimetry-part 4: CIE 1976 L* a* B* Colour Space.

Fisher, R.A., 1936. The use of multiple measurements in taxonomic problems. Annals of eugenics 7 (2), 179–188.

Gutmann, H.M., 2001. A radial basis function method for global optimization. J. Global Optim. 19 (3), 201–227.

Howard, L., Smith, R.T., Wagner, A.B., Villalon, B., Burns, E.E., 1994. Provitamin A and ascorbic acid content of fresh pepper cultivars (Capsicum annuum) and processed jalapenos. J. Food Sci. 59 (2), 362–365. https://doi.org/10.1111/j.1365-2621.1994.tb06967.x.

Ignat, T., Mizrach, A., Schmilovitch, Z.E., Felföldi, J., 2010. Bell pepper maturity determination by ultrasonic techniques. Prog. Agric. Eng. Sci. 6 (1), 17–34. https://doi.org/10.1556/progress.6.2010.2.

Ignat, T., Schmilovitch, Z., Feföldi, J., Bernstein, N., Steiner, B., Egozi, H., Hoffman, A., 2013. Nonlinear methods for estimation of maturity stage, total chlorophyll, and carotenoid content in intact bell peppers. Biosyst. Eng. 114 (4), 414–425. https://doi.org/10.1016/j.biosystemseng.2012.10.001.

Ignat, T., Alchanatis, V., Schmilovitch, Z.E., 2014. Maturity prediction of intact bell peppers by sensor fusion. Comput. Electron. Agric. 104, 9–17. https://doi.org/10.1016/j.compag.2014.03.006.

Kasampalis, D.S., Tsouvaltzis, P., Ntouros, K., Gertsis, A., Gitas, I., Moshou, D., Siomos, A.S., 2022. Nutritional composition changes in bell pepper as affected by the ripening stage of fruits at harvest or postharvest storage and assessed non-destructively. J. Sci. Food Agric. 102 (1), 445–454. https://doi.org/10.1002/jsfa.11375.

León-Chan, R.G., López-Meyer, M., Osuna-Enciso, T., Sañudo-Barajas, J.A., Heredia, J.B., León-Félix, J., 2017. Low temperature and ultraviolet-B radiation affect chlorophyll content and induce the accumulation of UV-B-absorbing and antioxidant compounds in bell pepper (Capsicum annuum) plants. Environ. Exp. Bot. 139, 143–151.

Lichtenthaler, H. K. (1987). [34] Chlorophylls and carotenoids: pigments of photosynthetic biomembranes. In Methods in Enzymology (Vol. vol. 148, pp. 350-382). Academic Press.

Logan, R. D., Scherrer, B., Senecal, J., Walton, N. S., Peerlinck, A., Sheppard, J. W., & Shaw, J. A. (2020). Hyperspectral imaging and machine learning for monitoring produce ripeness. In Sensing for Agriculture and Food Quality and Safety XII (Vol. vol. 11421, pp. 95-108). SPIE.

Mohebbi, M., Amiryousefi, M.R., Hasanpour, N., Ansarifar, E., 2012. Employing an intelligence model and sensitivity analysis to investigate some physicochemical properties of coated bell pepper during storage. Int. J. Food Sci. Technol. 47 (2), 299–305. https://doi.org/10.1111/j.1365-2621.2011.02839.x.

Ohta, N., & Robertson, A. (2006). Colorimetry: Fundamentals and Applications. John Wiley & Sons.

Paredes, A.C., Peche, J.Y., León, N., 2019. Index of carotenoids of bell pepper (Capsicum annuum) based on color measurement, using hyperspectral and digital images. Sci. Agropecu. 10 (4), 531–539. https://doi.org/10.17268/sci.agropecu.2019.04.10.

Pu, Y.Y., Feng, Y.Z., Sun, D.W., 2015. Recent progress of hyperspectral imaging on quality and safety inspection of fruits and vegetables: a review. Compr. Rev. Food Sci. Food Saf. 14 (2), 176–188. https://doi.org/10.1111/1541-4337.12123.

Schmilovitch, Z.E., Ignat, T., Alchanatis, V., Gatker, J., Ostrovsky, V., Felföldi, J., 2014. Hyperspectral imaging of intact bell peppers. Biosyst. Eng. 117, 83–93. https://doi.org/10.1016/j.biosystemseng.2013.07.003.

Thorlabs: https://www.thorlabs.com/thorproduct.cfm?partnumber=SLS201L accessed 1/June/2023.

Villaseñor-Aguilar, M.J., Bravo-Sánchez, M.G., Padilla-Medina, J.A., Vázquez-Vera, J.L., Guevara-González, R.G., García-Rodríguez, F.J., Barranco-Gutiérrez, A.I., 2020. A maturity estimation of bell pepper (Capsicum annuum L.) by artificial vision system for quality control. Appl. Sci. 10 (15), 5097. https://doi.org/10.3390/app10155097.

Wall, M.M., Waddell, C.A., Bosland, P.W., 2001. Variation in β-carotene and total carotenoid content in fruits of Capsicum. Hortscience 36 (4), 746–749.

Weston, L.A., Barth, M.M., 1997. Preharvest factors affecting postharvest quality of vegetables. Hortscience 32 (5), 812–816. https://doi.org/10.21273/HORTSCI.30.4.750F.

Weston, J., & Watkins, C. (1998). Multi-class Support Vector Machines (pp. 98-04). Technical Report CSD-TR-98-04, Department of Computer Science, Royal Holloway, University of London.

Yuan, Z., Ye, Y., Wei, L., Yang, X., Huang, C., 2021. Study on the optimization of hyperspectral characteristic bands combined with monitoring and visualization of pepper leaf SPAD value. Sensors 22 (1), 183. https://doi.org/10.3390/s22010183.

Zontov, Y.V., Rodionova, O.Y., Kucheryavskiy, S.V., Pomerantsev, A.L., 2020. PLS-DA–A MATLAB GUI tool for hard and soft approaches to partial least squares discriminant analysis. Chemometr. Intell. Lab. Syst. 203, 104064 https://doi.org/10.1016/j.chemolab.2020.104064.

– Resonon: web: https://resonon.com/Pika-L accessed 01/June/2023.